

Au₁₃(8e): A Secondary Block for Describing a Special Group of Liganded Gold Clusters Containing Icosahedral Au₁₃ Motifs

Wen Wu Xu^{1,2}, Xiao Cheng Zeng^{*2,3}, Yi Gao^{*1,4}

¹*Division of Interfacial Water and Key Laboratory of Interfacial Physics and Technology, Shanghai Institute of Applied Physics, Chinese Academy of Sciences, Shanghai 201800, China.*

²*Department of Chemistry, University of Nebraska-Lincoln, Lincoln, Nebraska 68588, USA.*

³*Collaborative Innovation Center of Chemistry for Energy Materials, University of Science and Technology of China, Hefei, Anhui 230026, China*

⁴*Shanghai Science Research Center, Chinese Academy of Sciences, Shanghai 201204, China*

**Correspondence Email: xzeng1@unl.edu, gaoyi@sinap.ac.cn*

Abstract

A grand unified model (GUM) (*Nat. Commun.* **7**, 13574 (2016)) has been proposed recently to understand structure anatomy and structural evolution of 71 liganded gold clusters reported in the literature. In GUM, the gold core of each liganded gold cluster can be viewed as packing of two types of elementary blocks, namely, triangular Au₃(2e) and tetrahedral Au₄(2e), and each elementary block is assigned to have 2e valence electrons (the duet rule). In this work, we introduce a secondary block, namely, the icosahedral Au₁₃ with 8e valence electrons, noted as Au₁₃(8e). The secondary block can be viewed as a combination of four elementary blocks. Using the secondary block Au₁₃(8e), structural anatomy of a special group of liganded gold nanoclusters containing icosahedral Au₁₃ motifs can be conveniently analyzed. Moreover, the structural evolution of experimentally synthesized clusters, [Au₁₃(PR₃)₁₀Cl₂]³⁺, [Au₂₅(PR₃)₁₀(SR)₅Cl₂]²⁺, and [Au₃₇(PR₃)₁₀(SR)₁₀Cl₂]¹⁺, can be elucidated. Notably, we found that the charges of [Au₁₃(PR₃)₁₀Cl₂]³⁺, [Au₂₅(PR₃)₁₀(SR)₅Cl₂]²⁺, and [Au₃₇(PR₃)₁₀(SR)₁₀Cl₂]¹⁺ decrease from +3 to +1 with increasing the number of secondary blocks of Au₁₃(8e) from 1 to 3. By extending this trend to higher number of secondary block Au₁₃(8e), a new cluster Au₄₉(PR₃)₁₀(SR)₁₅Cl₂ is predicted. Chemical and thermal stability of this newly predicted cluster is examined, suggesting likelihood of its synthesis in the laboratory.

1. Introduction

Ligand-protected gold (Au) clusters have attracted considerable interests due to their broad applications in electrochemistry, nanocatalysis and bioengineering.[1-4] From 1970s to the present, a large number of liganded gold nanoclusters have been synthesized and their structures have been determined via X-ray crystallography [5-10]

or predicted by density functional theory (DFT) computation.[11-17] Although total structural determination and prediction of numerous ligand-protected gold nanoclusters have been accomplished, understanding of their structural stabilities and evolution of many seemingly-unrelated structures of the liganded gold nanoclusters remains to be an active area of research. In 1970s, the Wade-Mingos electron-counting rule was proposed and later employed in the cluster chemistry.[18,19] However, this rule of thumb cannot fully describe ligand-protected Au nanoclusters.[20] In 2008, Walter and Häkkinen *et al.* proposed the superatom complex (SAC) model to explain high stabilities of some spherical ligand-protected Au nanoclusters with total count of valence electrons of 2, 8, 18, 34, 58 (electronic shell closing) on basis of the jellium model.[21] Later, Cheng *et al.* developed a super valence bond (SVB) model [22] and a superatom network (SAN) model [23] to interpret high stabilities of certain nonspherical thiolate-protected Au nanoclusters based on the adaptive natural density partitioning (AdNDP) analysis.[24] A key concept in SAN model is the core of Au nanoclusters can be viewed as a network of n -centered two-electron ($n = 2-6$) superatoms, originally developed to describe some small-sized Au clusters by Sergeeva and Boldyrev.[25] Mingos analyzed some ligand-protected Au nanoclusters containing vertex, edge, or face-sharing icosahedral or cuboctahedra Au_{13} units, by using the notion of the united atom model for diatomic molecules (i.e., F_2 , O_2 , N_2 etc.).[26] Very recently, the Borromean-ring diagrams [27] were utilized by Pradeep, Whetten and coworkers to analyze high stabilities of $[Au_{25}(SR)_{18}]^{1-}$, [9-11] $Au_{38}(SR)_{24}$, [28] and $Au_{102}(SR)_{44}$. [6] Again, because of the wide variety of ligand-protected Au nanoclusters with different core morphologies, protection ligands, and number of valence electrons, none of these models can offer a unified description of their structure anatomy, structural stabilities and evolution.

Recently, a grand unified model (GUM) has been proposed to gain fundamental understanding of a plethora of complex and seemingly-unrelated structures of liganded gold clusters.[29] In GUM, depending on the connected chemical group of protection ligands, gold atoms on surface of the gold core can be assigned to three possible valence states (in names of three flavors), i.e., bottom ($1e$), middle ($0.5e$), and top ($0e$) flavor. The gold cores of all 71 ligand-protected clusters reported in the literature can be universally viewed as packing of two types of elementary blocks: triangular Au_3 and tetrahedral Au_4 , each satisfying the duet rule [noted as $Au_3(2e)$ and $Au_4(2e)$]. Such a generic rule of thumb can be used to characterize the stabilities and structural evolution of liganded gold clusters. Among the 71 ligand-protected clusters, there is a special group of liganded gold nanoclusters all containing one or several icosahedral Au_{13} motifs, such as $[Au_{13}(PR_3)_{10}Cl_2]^{3+}$, [30] $[Au_{13}(dppe)_5Cl_2]^{3+}$, [31] $Au_{16}(AsPh_3)_8Cl_6$, [32] $[Au_{19}(C\equiv CR)_9(Hdppa)_3]^{2+}$, [33] $Au_{20}(PP_3)_4Cl_4$, [34] $[Au_{25}(PR_3)_{10}(SR)_5Cl_2]^{2+}$, [35] $[Au_{25}(SR)_{18}]^{1-}$, [9-11] $[Au_{37}(PR_3)_{10}(SR)_{10}Cl_2]^{1+}$, [36] and $Au_{38}(SR)_{24}$. [28,37] For these liganded clusters, according to the electron counting protocols for effective detachment of ligands in GUM, each icosahedral Au_{13} motif is assigned to have $8e$ valence electrons $[Au_{13}(8e)]$. In fact, each icosahedral Au_{13} motif

can be viewed as packing of four elementary blocks. For example, the $\text{Au}_{13}(8e)$ in $[\text{Au}_{25}(\text{SR})_{18}]^{1-}$ consists of two elementary blocks of $\text{Au}_3(2e)$ and two $\text{Au}_4(2e)$, as shown in Figure S1. The AdNDP analysis (Figure S2) also confirms that the $\text{Au}_{13}(8e)$ can be decomposed into four elementary blocks. Note that this decomposition is not intended to reflect the electronic structure of the Au_{13} core at the molecular level (Figure S3) but simply to indicate that the $8e$ valence electrons of $\text{Au}_{13}(8e)$ can be viewed as a sum of four pairs of valence electrons of the four elementary blocks. The elementary blocks $\text{Au}_3(2e)$ and $\text{Au}_4(2e)$ can be also viewed as electron shell closure species, in analogue of that of the stable He atom. Likewise, $\text{Au}_{13}(8e)$ can be viewed as an electron shell closure species, in analogue of that of the stable Ne atom. As such, the $\text{Au}_{13}(8e)$ may be regarded as a secondary block (or coarse-grained block) to constitute the gold cores of a special group of liganded gold clusters. As such, 91 variants of valence states (named as $I_1 - I_{91}$) for the secondary block $\text{Au}_{13}(8e)$ can be identified (see Table S1). In addition, the structural evolution of $[\text{Au}_{13}(\text{PR}_3)_{10}\text{Cl}_2]^{3+}$, $[\text{Au}_{25}(\text{PR}_3)_{10}(\text{SR})_5\text{Cl}_2]^{2+}$, and $[\text{Au}_{37}(\text{PR}_3)_{10}(\text{SR})_{10}\text{Cl}_2]^{1+}$ can be analyzed more conveniently on the basis of the secondary block $\text{Au}_{13}(8e)$. Furthermore, a new cluster $\text{Au}_{49}(\text{PR}_3)_{10}(\text{SR})_{15}\text{Cl}_2$ is predicted based on the structure trend obtained with the three experimentally synthesized clusters.

2. Computational methods

Structural optimizations of the liganded gold clusters were performed using density functional theory (DFT) methods implemented in the Gaussian 09 program package [38]. The the M06L functional [39] and the all-electron basis set 6-31G* for H, P, S, and Cl, effective-core basis set LANL2DZ for Au were selected. *Ab initio* molecular dynamics simulation was performed in the canonical ensemble at a finite temperature of 355 K using DFT method implemented in the CP2K package.[40,41] The Nose-Hoover thermostat and a time step of 1 fs were employed. The exchange correlation potential was described by the generalized-gradient approximation (GGA) with the spin-polarized functional of Perdew-Burke-Ernzerh (PBE).[42] Wavefunctions were expanded in triple- ζ Gaussian basis sets with an auxiliary plane-wave basis and a cutoff energy of 300 Ry. Core electrons were treated by scalar relativistic norm-conserving pseudopotentials with 11, 7, 6, 5, and 1 valence electrons of Au, Cl, S, P, and H, respectively.[43,44] Brillouin zone integration was undertaken with using a reciprocal-space mesh consisting of only the Γ -point. The $-R$ group is replaced by $-H$ to significantly lower computational cost.

3. Results and discussions

Based on the 91 variants of valence states of the secondary block $\text{Au}_{13}(8e)$, $I_1 - I_{91}$, as presented in Table S1, the representative valence states for the secondary blocks of $\text{Au}_{13}(8e)$ in $[\text{Au}_{13}(\text{PR}_3)_{10}\text{Cl}_2]^{3+}$,[30] $[\text{Au}_{13}(\text{dppe})_5\text{Cl}_2]^{3+}$,[31] $\text{Au}_{16}(\text{AsPh}_3)_8\text{Cl}_6$,[32] $[\text{Au}_{19}(\text{C}\equiv\text{CR})_9(\text{Hdppa})_3]^{2+}$,[33] $\text{Au}_{20}(\text{PP}_3)_4\text{Cl}_4$,[34] $[\text{Au}_{25}(\text{PR}_3)_{10}(\text{SR})_5\text{Cl}_2]^{2+}$,[35]

$[\text{Au}_{25}(\text{SR})_{18}]^{1-}$,^[9-11] $[\text{Au}_{37}(\text{PR}_3)_{10}(\text{SR})_{10}\text{Cl}_2]^{1+}$,^[36] and $\text{Au}_{38}(\text{SR})_{24}$ ^[28,37] clusters are shown in Figure 1.

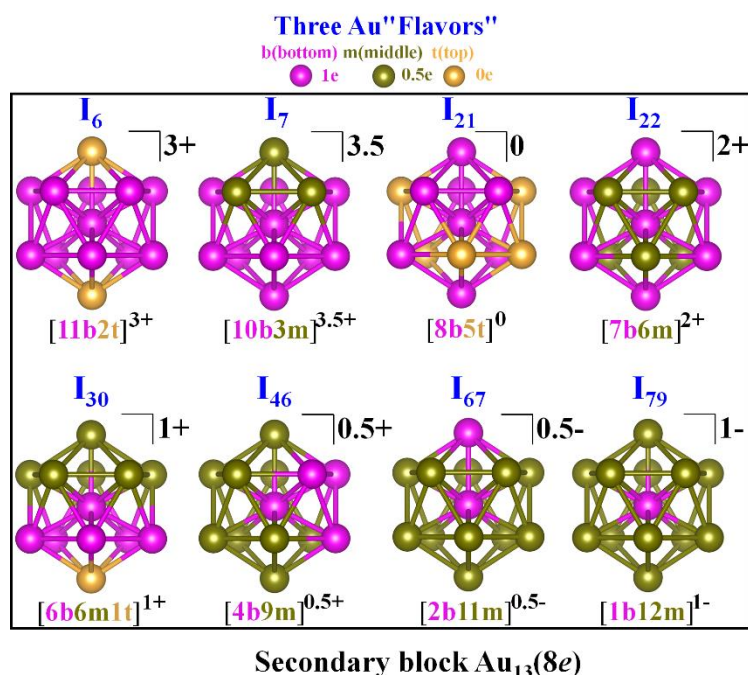


Figure 1. 8 of the 91 variants ($I_1 - I_{91}$) of valence states for the secondary block $\text{Au}_{13}(8e)$ in $[\text{Au}_{13}(\text{PR}_3)_{10}\text{Cl}_2]^{3+}$, $[\text{Au}_{13}(\text{dppe})_5\text{Cl}_2]^{3+}$, $\text{Au}_{16}(\text{AsPh}_3)_8\text{Cl}_6$, $[\text{Au}_{19}(\text{C}\equiv\text{CR})_9(\text{Hdppa})_3]^{2+}$, $\text{Au}_{20}(\text{PP}_3)_4\text{Cl}_4$, $[\text{Au}_{25}(\text{PR}_3)_{10}(\text{SR})_5\text{Cl}_2]^{2+}$, $[\text{Au}_{25}(\text{SR})_{18}]^{1-}$,⁹⁻¹¹ $[\text{Au}_{37}(\text{PR}_3)_{10}(\text{SR})_{10}\text{Cl}_2]^{1+}$, and $\text{Au}_{38}(\text{SR})_{24}$ clusters. Color code: Au – magenta (“bottom flavor”), dark yellow (“middle flavor”), and yellow (“top flavor”).

Next, two prototype structures are used as two examples to analyze the valence state of the secondary block $\text{Au}_{13}(8e)$. The first is $[\text{Au}_{25}(\text{SR})_{18}]^{1-}$,^[9-11] a cluster widely investigated experimentally and theoretically.^[45,46] As shown in Figure 2a, the icosahedral Au_{13} core of $[\text{Au}_{25}(\text{SR})_{18}]^{1-}$ is protected by six $[\text{SR-Au-SR-Au-RS}]$ staple motifs. According to electron counting protocols of GUM, each of the two surface gold atoms in the core bonded with SR is assigned to transfer 0.5e valence electron to the staple motif.²⁹ Thus, each of the 12 surface gold atoms of the icosahedral Au_{13} core possesses 0.5e valence electron. Since the central gold atom of the icosahedral Au_{13} core has 1e valence electron and the net charge of $[\text{Au}_{25}(\text{SR})_{18}]^{1-}$ is -1, the total valence electrons of the icosahedral Au_{13} core is $12 \times 0.5e + 1e + 1e = 8e$, and the icosahedral Au_{13} core is in the I_{79} valence state. The second prototype structure considered is $\text{Au}_{16}(\text{AsPh}_3)_8\text{Cl}_6$.^[32] It can be seen from Figure 2b and Figure 2c that the Au_{16} core $\text{Au}_{16}(\text{AsPh}_3)_8\text{Cl}_6$ can be viewed as an icosahedral Au_{13} motif combined with a triangular Au_3 motif. Each gold atom bonded with Cl/ AsR_3 group possesses 1e/0e valence electron. The total number of valence electrons of the icosahedral Au_{13} motif and triangular Au_3 are 10e. Thus, the Au_{16} core in

$\text{Au}_{16}(\text{AsPh}_3)_8\text{Cl}_6$ can be decomposed as one secondary block $\text{Au}_{13}(8e)$ in the I_{21} valence state and one elementary block $\text{Au}_3(2e)$ in the Δ_4 valence state.

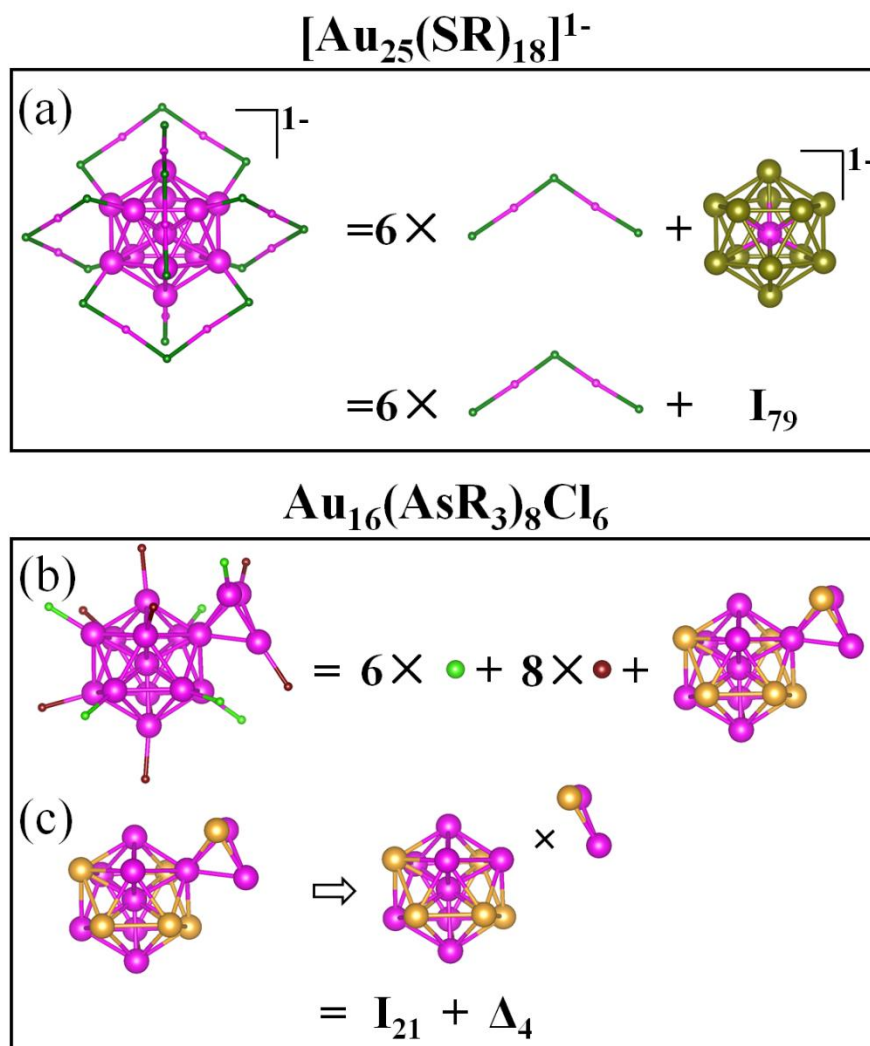


Figure 2. A structural decomposition of $[\text{Au}_{25}(\text{SR})_{18}]^{1-}$ (a) and $\text{Au}_{16}(\text{AsPh}_3)_8\text{Cl}_6$ (b and c). Au – magenta (“bottom flavor”), dark yellow (“middle flavor”), and yellow (“top flavor”); SR – dark green; Cl – light green; AsR_3 – wine. The R groups are omitted for clarity.

In Figure 3, structural decompositions of $[\text{Au}_{13}(\text{PR}_3)_{10}\text{Cl}_2]^{3+}$,^[30] $[\text{Au}_{25}(\text{PR}_3)_{10}(\text{SR})_5\text{Cl}_2]^{2+}$,^[35] and $[\text{Au}_{37}(\text{PR}_3)_{10}(\text{SR})_{10}\text{Cl}_2]^{1+}$ ^[36] are displayed. It can be seen that the icosahedral Au_{13} core of $[\text{Au}_{13}(\text{PR}_3)_{10}\text{Cl}_2]^{3+}$ is in the I_6 valence state (Figure 3a). The Au_{25} core in the $[\text{Au}_{25}(\text{PR}_3)_{10}(\text{SR})_5\text{Cl}_2]^{2+}$ cluster can be viewed as two icosahedral Au_{13} motifs fused together by sharing one Au atom (Figure 3b). Each icosahedral Au_{13} motif, with 8 valence electrons, is in the I_{30} valence state (Figure 3c). Likewise, the Au_{37} core of $[\text{Au}_{37}(\text{PR}_3)_{10}(\text{SR})_{10}\text{Cl}_2]^{1+}$ cluster can be viewed as three icosahedral Au_{13} motifs fused together by sharing two Au atoms (Figure 3d). Specifically, the three secondary blocks $\text{Au}_{13}(8e)$ are in the I_{30} , I_{30} , and I_{79} valence

state, respectively, giving rise to totally 24 valence electrons for the core of $[\text{Au}_{37}(\text{PR}_3)_{10}(\text{SR})_{10}\text{Cl}_2]^{1+}$ cluster (Figure 3e).

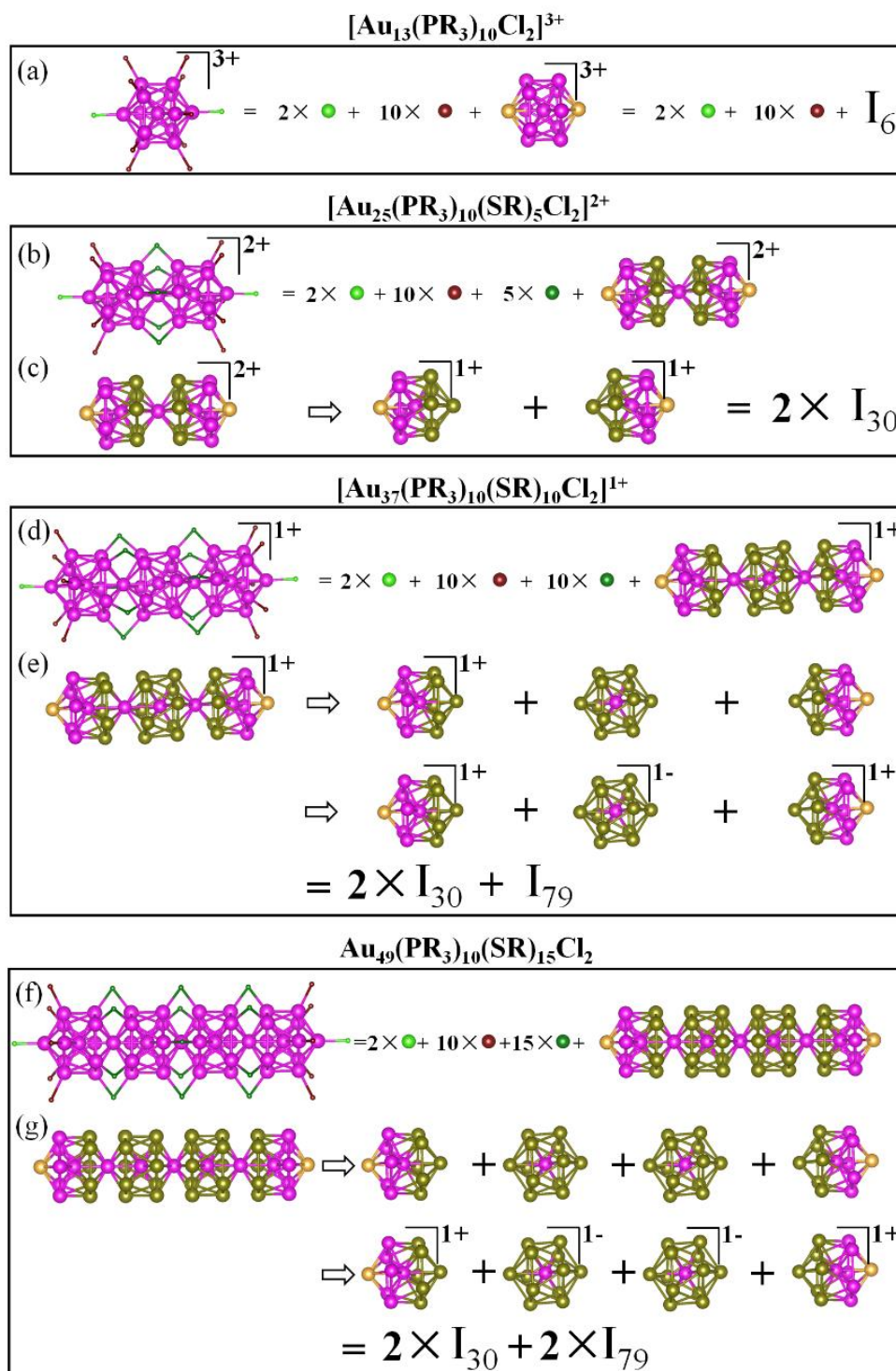


Figure 3. A structural decomposition of $[\text{Au}_{13}(\text{PR}_3)_{10}\text{Cl}_2]^{3+}$ (a), $[\text{Au}_{25}(\text{PR}_3)_{10}(\text{SR})_5\text{Cl}_2]^{2+}$ (b and c), $[\text{Au}_{37}(\text{PR}_3)_{10}(\text{SR})_{10}\text{Cl}_2]^{1+}$ (d and e), and $\text{Au}_{49}(\text{PR}_3)_{10}(\text{SR})_{15}\text{Cl}_2$ (f and g). Color code: Au – magenta (“bottom flavor”), dark yellow (“middle flavor”), and yellow (“top flavor”); SR – dark green; Cl – light green; PR_3 – wine. The R groups are omitted for clarity.

It should be noted that the charges of $[\text{Au}_{13}(\text{PR}_3)_{10}\text{Cl}_2]^{3+}$, $[\text{Au}_{25}(\text{PR}_3)_{10}(\text{SR})_5\text{Cl}_2]^{2+}$, and $[\text{Au}_{37}(\text{PR}_3)_{10}(\text{SR})_{10}\text{Cl}_2]^{1+}$ decrease from +3 to +1 with increasing the number of the secondary blocks of $\text{Au}_{13}(8e)$, as shown in Table 1. This trend suggests that the adjustment of the overall charge state is correlated with allowing each icosahedral Au_{13} motif to have with 8 valence electrons. If this empirical trend can be extended to a larger-sized cluster whose gold core has four secondary blocks of $\text{Au}_{13}(8e)$, a neutral $\text{Au}_{49}(\text{PR}_3)_{10}(\text{SR})_{15}\text{Cl}_2$ cluster with 32 valence electrons can be predicted (see Table 1 and Figure 3f). Here, the four secondary blocks $\text{Au}_{13}(8e)$ are in the I_{30} , I_{30} , I_{79} , and I_{79} valence state (Figure 3g), respectively. This newly predicted $\text{Au}_{49}(\text{PR}_3)_{10}(\text{SR})_{15}\text{Cl}_2$ cluster exhibits a computed HOMO-LUMO gap of 0.79 eV, suggesting that this cluster is likely chemically stable. On the other hand, the HOMO-LUMO gaps for this series of clusters suggest that the chemical stabilities from $[\text{Au}_{13}(\text{PR}_3)_{10}\text{Cl}_2]^{3+}$ to $\text{Au}_{49}(\text{PR}_3)_{10}(\text{SR})_{15}\text{Cl}_2$ may become weaker with increasing the number of secondary blocks $\text{Au}_{13}(8e)$. Lastly, 10 ps *ab initio* molecular dynamics (AIMD) simulation performed for the $\text{Au}_{49}(\text{PR}_3)_{10}(\text{SR})_{15}\text{Cl}_2$ cluster suggested that the cluster may be thermally stable at 355 K (Figure 4).

Table 1. Computed properties of $[\text{Au}_{13}(\text{PR}_3)_{10}\text{Cl}_2]^{3+}$, $[\text{Au}_{25}(\text{PR}_3)_{10}(\text{SR})_5\text{Cl}_2]^{2+}$, $[\text{Au}_{37}(\text{PR}_3)_{10}(\text{SR})_{10}\text{Cl}_2]^{1+}$, and $\text{Au}_{49}(\text{PR}_3)_{10}(\text{SR})_{15}\text{Cl}_2$. * denotes a predicted structure based on GUM.

	Charge	Number of valence electrons	Number of $\text{Au}_{13}(8e)$	HOMO-LUMO gap/eV
$[\text{Au}_{13}(\text{PR}_3)_{10}\text{Cl}_2]^{3+}$	+3	8	1	1.96
$[\text{Au}_{25}(\text{PR}_3)_{10}(\text{SR})_5\text{Cl}_2]^{2+}$	+2	16	2	1.31
$[\text{Au}_{37}(\text{PR}_3)_{10}(\text{SR})_{10}\text{Cl}_2]^{1+}$	+1	24	3	0.90
$\text{Au}_{49}(\text{PR}_3)_{10}(\text{SR})_{15}\text{Cl}_2$ *	0	32	4	0.79

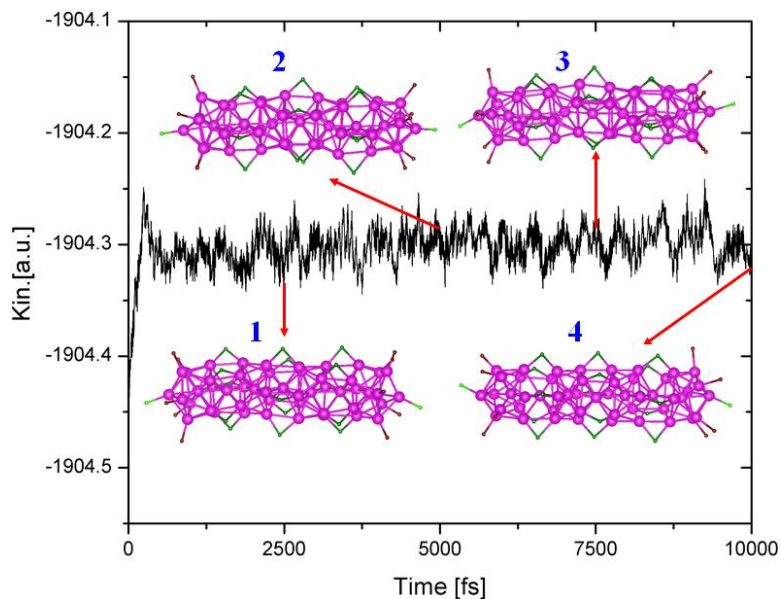


Figure 4. Computed kinetic energy (Kin) vs simulation time in an *ab initio* molecular dynamics simulation of the $\text{Au}_{49}(\text{PH}_3)_{10}(\text{SH})_{15}\text{Cl}_2$ cluster at 355 K. 1, 2, 3, and 4 correspond to the snapshot at 2.5, 5, 7.5, and 10 ps, respectively. Color code: Au – magenta; SR – dark green; PR_3 – wine. The H atoms are omitted for clarity.

4 Conclusions

We have proposed that the Au_{13} with 8 valence electrons can be conveniently viewed as a secondary block to describe structure anatomy and structural evolution of a special group of liganded gold clusters containing single or multiple icosahedral Au_{13} motifs. Such a secondary block, noted as $\text{Au}_{13}(8e)$, can exhibit 91 variants of valence states ($I_1 - I_{91}$) due to three possible “flavors” [bottom ($1e$), middle ($0.5e$), and top ($0e$)] of gold atoms. The structural evolution from $[\text{Au}_{13}(\text{PR}_3)_{10}\text{Cl}_2]^{3+}$ to $[\text{Au}_{25}(\text{PR}_3)_{10}(\text{SR})_5\text{Cl}_2]^{2+}$ and $[\text{Au}_{37}(\text{PR}_3)_{10}(\text{SR})_{10}\text{Cl}_2]^{1+}$ is illustrated with the increasing number of the secondary blocks. We found that the charges of $[\text{Au}_{13}(\text{PR}_3)_{10}\text{Cl}_2]^{3+}$, $[\text{Au}_{25}(\text{PR}_3)_{10}(\text{SR})_5\text{Cl}_2]^{2+}$, and $[\text{Au}_{37}(\text{PR}_3)_{10}(\text{SR})_{10}\text{Cl}_2]^{1+}$ decrease from +3 to +1 with the increase of the number of secondary blocks $\text{Au}_{13}(8e)$ from 1 to 3. Based on this trend, a new cluster, $\text{Au}_{49}(\text{PR}_3)_{10}(\text{SR})_{15}\text{Cl}_2$ with four secondary blocks $\text{Au}_{13}(8e)$, is predicted. This cluster seems to have high chemical and thermal stability, thereby may be synthesized in the laboratory. The introduction of secondary block $\text{Au}_{13}(8e)$ into GUM appears to be a convenient supplement to understand a special group of liganded gold clusters containing icosahedral Au_{13} motifs, and thus may be exploited for predicting new liganded gold clusters by design.

Acknowledgements

W.W.X. is supported by National Natural Science Foundation of China (11504396). Y.G. is supported by the start-up funding from Shanghai Institute of Applied Physics, Chinese Academy of Sciences (Y290011011), National Natural Science Foundation

of China (21273268, 11574340), ‘Hundred People Project’ from Chinese Academy of Sciences and CAS-Shanghai Science Research Center (CAS-SSRC-YJ-2015-01). X.C.Z. is supported by a grant from Nebraska Center for Energy Sciences Research and a Qian-ren B (One Thousand Talent Plan B) summer research fund from USTC, and by a State Key R&D Fund of China (2016YFA0200604) to USTC. The computational resources utilized in this research were provided by Shanghai Supercomputer Center, National Supercomputing Center in Tianjin and Shenzhen, special program for applied research on super computation of the NSFC-Guangdong joint fund (the second phase) and NC3 computer facility in University of Nebraska-Lincoln.

References

- [1] D. M. P. Mingos, T. Slee, L. Zhenyang, *Chem. Rev.* 90(1990) 383.
- [2] R. W. Murray, *Chem. Rev.* 108 (2008) 2688.
- [3] H. Qian, M. Zhu, Z. Wu, R. Jin, *Acc. Chem. Res.* 45(2012) 1470.
- [4] H. Häkkinen, *Nat. Chem.* 4(2012) 443.
- [5] R. Jin, C. Zeng, M. Zhou, Y. Chen, *Chem. Rev.* 116(2016) 10346.
- [6] P. D. Jadzinsky, G. Calero, C. J. Ackerson, D. A. Bushnell, R. D. Kornberg, *Science* 2007, 318, 430-433.
- [7] C. Zeng, Y. Chen, K. Kirschbaum, K. Appavoo, M. Y. Sfeir, R. Jin, *Sci. Adv.* 2015, 1, e1500045.
- [8] C. Zeng, Y. Chen, K. Kirschbaum, K. J. Lambright, R. Jin, *Science* 354(2016) 1580.
- [9] M. Zhu, C. M. Aikens, F. J. Hollander, G. C. Schatz, R. Jin, *J. Am. Chem. Soc.* 130(2008) 5883.
- [10] M. W. Heaven, A. Dass, P. S. White, K. M. Holt, R. W. Murray, *J. Am. Chem. Soc.* 130(2008) 3754.
- [11] J. Akola, M. Walter, R. L. Whetten, H. Häkkinen, H. Grönbeck, *J. Am. Chem. Soc.* 130(2008) 3756.
- [12] Y. Pei, Y. Gao, X. C. Zeng, *J. Am. Chem. Soc.* 130(2008) 7830.
- [13] Y. Pei, Y. Gao, N. Shao, X. C. Zeng, *J. Am. Chem. Soc.* 131(2009) 13619.
- [14] Y. Pei, R. Pal, C. Liu, Y. Gao, Z. Zhang, X. C. Zeng, *J. Am. Chem. Soc.* 134(2012) 3015.
- [15] S. Malola, L. Lehtovaara, S. Knoppe, K. Hu, R. E. Palmer, T. B ürgi, H. Häkkinen, *J. Am. Chem. Soc.* 134(2012) 19560.
- [16] D. Jiang, S. H. Overbury, S. Dai, *J. Am. Chem. Soc.* 135(2013) 8786.
- [17] W. W. Xu, Y. Gao, X. C. Zeng, *Sci. Adv.* 1(2015) e1400211.
- [18] K. Wade, *J. Chem. Soc. D* (1972) 792.
- [19] D. M. P. Mingos, *Nature Phys. Sci.* 236(1972) 99.
- [20] D. M. P. Mingos, *J. Chem. Soc., Dalton Trans.* (1976) 1163.
- [21] M. Walter, J. Akola, O. Lopez-Acevedo, P. D. Jadzinsky, G. Calero, C. J. Ackerson, R. L. Whetten, H. Grönbeck, H. Häkkinen, *Proc. Natl. Acad. Sci.* 105(2008) 9157.

- [22] L. Cheng, C. Ren, X. Zhang, J. Yang, *Nanoscale* 5(2013) 1475.
- [23] L. Cheng, Y. Yuan, X. Zhang, J. Yang, *Angew. Chem. Int. Ed.* 52(2013) 9035.
- [24] D. Y. Zubarev, A. I. Boldyrev, *Phys. Chem. Chem. Phys.* 10(2008) 5207.
- [25] A. P. Sergeeva, A. I. Boldyrev *J. Clust. Sci.* 22(2011) 321.
- [26] D. M. P. Mingos, *Dalton Trans.* 44(2015) 6680.
- [27] G. Natarajan, A. Mathew, Y. Negishi, R. L. Whetten, T. Pradeep, *J. Phys. Chem. C* 119(2015) 27768.
- [28] H. Qian, W. T. Eckenhoff, Y. Zhu, T. Pintauer R. Jin, *J. Am. Chem. Soc.* 132(2010) 8280.
- [29] W. W. Xu, B. Zhu, X. C. Zeng, Y. Gao, *Nat. Commun.* 7(2016) 13574.
- [30] C. E. Briant, B. R. C. Tobald, J. W. White, L. K. Bell, D. M. P. Mingos, *J. Chem. Soc. Chem. Commun.* 5(1981) 201.
- [31] Y. Shichibu, K. Konishi, *Small* 6(2010) 1216.
- [32] M. Richter, J. Z. Strähle, *Anorg. Allg. Chem.* 627(2001) 918.
- [33] X. Wan, Q. Tang, S. Yuan, D. Jiang, Q. M. Wang, *J. Am. Chem. Soc.* 137(2015) 652.
- [34] X. Wan, S. Yuan, Z. Lin, Q. M. Wang, *Angew. Chem. Int. Ed.* 53(2014) 2923
- [35] Y. Shichibu, Y. Negishi, T. Watanabe, N. K. Chaki, H. Kawaguchi, T. Tsukuda, *J. Phys. Chem. C* 111(2007) 7845.
- [36] R. Jin, C. Liu, S. Zhao, A. Das, H. Xing, C. Gayathri, Y. Xing, N. L. Rosi, R. R. Gil, R. Jin, *ACS Nano* 9(2015) 8530.
- [37] S. Tian, Y. Li, M. Li, J. Yuan, J. Yang, Z. Wu, R. Jin, *Nat. Commun.* 6(2015) 8667.
- [38] M. J. Frisch, G. W. Trucks, H. B. Schlegel, G. E. Scuseria, M. A. Robb, J. R. Cheeseman, G. Scalmani, V. Barone, B. Mennucci, G. A. Petersson, H. Nakatsuji, M. Caricato, X. Li, H. P. Hratchian, A. F. Izmaylov, J. Bloino, G. Zheng, J. L. Sonnenberg, M. Hada, M. Ehara, K. Toyota, R. Fukuda, J. Hasegawa, M. Ishida, T. Nakajima, Y. Honda, O. Kitao, H. Nakai, T. Vreven, J. A. Montgomery, J. E. Peralta, F. Ogliaro, M. Bearpark, J. J. Heyd, E. Brothers, K. N. Kudin, V. N. Staroverov, R. Kobayashi, J. Normand, K. Raghavachari, A. Rendell, J. C. Burant, S. S. Iyengar, J. Tomasi, M. Cossi, N. Rega, J. M. Millam, M. Klene, J. E. Knox, J. B. Cross, V. Bakken, C. Adamo, J. Jaramillo, R. Gomperts, R. E. Stratmann, O. Yazyev, A. J. Austin, R. Cammi, C. Pomelli, J. W. Ochterski, R. L. Martin, K. Morokuma, V. G. Zakrzewski, G. A. Voth, P. Salvador, J. J. Dannenberg, S. Dapprich, A. D. Daniels, Ö. Farkas, J. B. Foresman, J. V. Ortiz, J. Cioslowski, D. J. Fox, *Gaussian 09*, Gaussian, Inc., Wallingford, CT, 2009.
- [39] Y. Zhao, D. G. Truhlar, *Theor. Chem. Acc.* 120(2008) 215.
- [40] G. Lippert, J. Hutter, M. Parrinello, *Theor. Chem. Acc.* 103(1999) 124.
- [41] J. VandeVondele, M. Krack, F. Mohamed, M. Parrinello, T. Chassaing, J. Hutter, *Comput. Phys. Commun.* 167(2005) 103.
- [42] J. P. Perdew, K. Burke, M. Ernzerhof, *Phys. Rev. Lett.* 77(1996) 3865.
- [43] S. Goedecker, M. Teter, J. Hutter, *Phys. Rev. B* 54(1996) 1703.
- [44] M. Krack, *Theor. Chem. Acc.* 114(2005) 145.

[45]G. Li, R. Jin, *Acc. Chem. Res.* 46(2013) 1749.

[46]C. Liu, S. Lin, Y. Pei, X. C. Zeng, *J. Am. Chem. Soc.* 135(2013) 18067.

Supporting Information

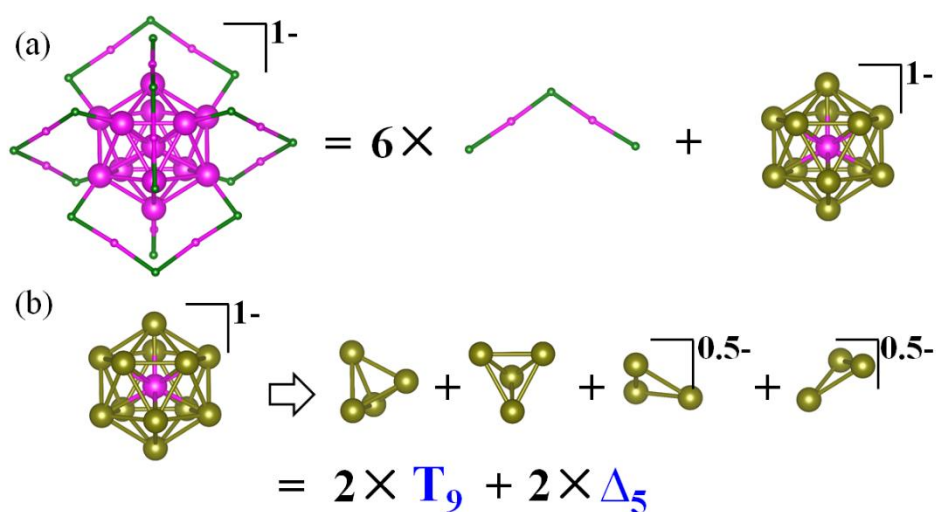


Figure S1. A structural decomposition of $[\text{Au}_{25}(\text{SR})_{18}]^{1-}$ (a and b) into four elementary blocks. Au – magenta (“bottom flavor”) and dark yellow (“middle flavor”); SR – dark green. The R groups are omitted for clarity.

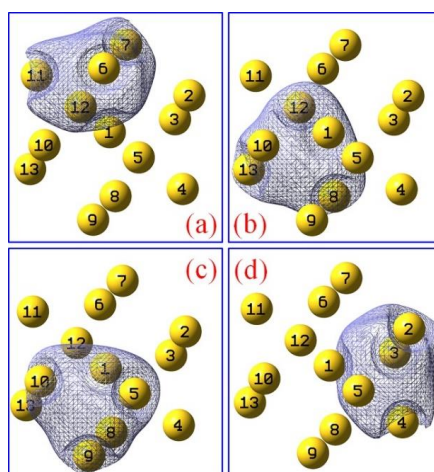


Figure S2. AdNDP analysis of the secondary block $\text{Au}_{13}(8e)$. The occupation number of the four elementary blocks (blue mesh) $\text{Au}_4(2e)$ in (a), (b), (c), and (d) are 1.63. The numbers 1-13 denote the 13 gold atoms. Color code: Au – yellow.

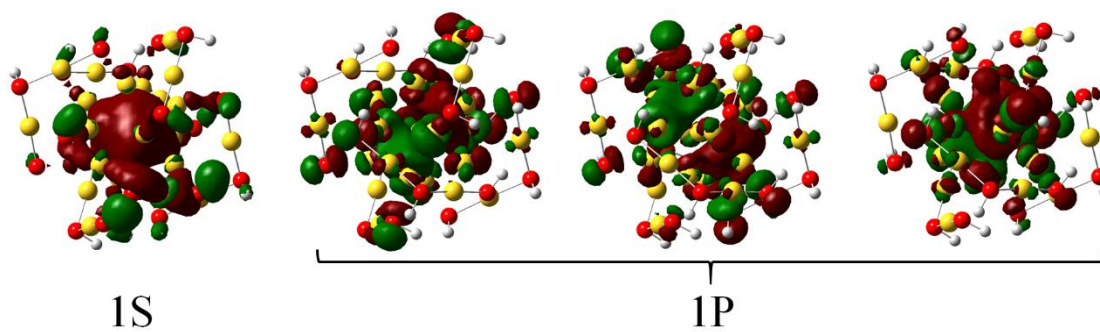


Figure S3. Computed delocalized occupied orbitals (1S and 1P) of $[\text{Au}_{25}(\text{SR})_{18}]^{1-}$. Color code: Au – yellow; S – red; H – white.

Table S1. 91 variants ($I_1 - I_{91}$) of valence states for the secondary block $Au_{13}(8e)$. b, m, and t denote bottom flavor ($1e$), middle flavor ($0.5e$), and top flavor ($0e$), respectively.

I_1	$[13b]^{5+}$	I_2	$[12b1m]^{4.5+}$	I_3	$[12b1t]^{4+}$
I_4	$[11b2m]^{4+}$	I_5	$[11b1m1t]^{3.5+}$	I_6	$[11b2t]^{3+}$
I_7	$[10b3m]^{3.5+}$	I_8	$[10b2m1t]^{3+}$	I_9	$[10b1m2t]^{2.5+}$
I_{10}	$[10b3t]^{2+}$	I_{11}	$[9b4m]^{3+}$	I_{12}	$[9b3m1t]^{2.5+}$
I_{13}	$[9b2m2t]^{2+}$	I_{14}	$[9b1m3t]^{1.5+}$	I_{15}	$[9b4t]^{1+}$
I_{16}	$[8b5m]^{2.5+}$	I_{17}	$[8b4m1t]^{2+}$	I_{18}	$[8b3m2t]^{1.5+}$
I_{19}	$[8b2m3t]^{1+}$	I_{20}	$[8b1m4t]^{0.5+}$	I_{21}	$[8b5t]^0$
I_{22}	$[7b6m]^{2+}$	I_{23}	$[7b5m1t]^{1.5+}$	I_{24}	$[7b4m2t]^{1+}$
I_{25}	$[7b3m3t]^{0.5+}$	I_{26}	$[7b2m4t]^0$	I_{27}	$[7b1m5t]^{0.5-}$
I_{28}	$[7b6t]^{1-}$	I_{29}	$[6b7m]^{1.5+}$	I_{30}	$[6b6m1t]^{1+}$
I_{31}	$[6b5m2t]^{0.5+}$	I_{32}	$[6b4m3t]^0$	I_{33}	$[6b3m4t]^{0.5-}$
I_{34}	$[6b2m5t]^{1-}$	I_{35}	$[6b1m6t]^{1.5-}$	I_{36}	$[6b7t]^{2-}$
I_{37}	$[5b8m]^{1+}$	I_{38}	$[5b7m1t]^{0.5+}$	I_{39}	$[5b6m2t]^0$
I_{40}	$[5b5m3t]^{0.5-}$	I_{41}	$[5b4m4t]^{1-}$	I_{42}	$[5b3m5t]^{1.5-}$
I_{43}	$[5b2m6t]^{2-}$	I_{44}	$[5b1m7t]^{2.5-}$	I_{45}	$[5b8t]^{3-}$
I_{46}	$[4b9m]^{0.5+}$	I_{47}	$[4b8m1t]^0$	I_{48}	$[4b7m2t]^{0.5-}$
I_{49}	$[4b6m3t]^{1-}$	I_{50}	$[4b5m4t]^{1.5-}$	I_{51}	$[4b4m5t]^{2-}$
I_{52}	$[4b3m6t]^{2.5-}$	I_{53}	$[4b2m7t]^{3-}$	I_{54}	$[4b1m8t]^{3.5-}$
I_{55}	$[4b9t]^{4-}$	I_{56}	$[3b10m]^0$	I_{57}	$[3b9m1t]^{0.5-}$
I_{58}	$[3b8m2t]^{1-}$	I_{59}	$[3b7m3t]^{1.5-}$	I_{60}	$[3b6m4t]^{2-}$
I_{61}	$[3b5m5t]^{2.5-}$	I_{62}	$[3b4m6t]^{3-}$	I_{63}	$[3b3m7t]^{3.5-}$
I_{64}	$[3b2m8t]^{4-}$	I_{65}	$[3b1m9t]^{4.5-}$	I_{66}	$[3b10t]^{5-}$

I₆₇	$[2b11m]^{0.5-}$	I₆₈	$[2b10m1t]^{1-}$	I₆₉	$[2b9m2t]^{1.5-}$
I₇₀	$[2b8m3t]^{2-}$	I₇₁	$[2b7m4t]^{2.5-}$	I₇₂	$[2b6m5t]^{3-}$
I₇₃	$[2b5m6t]^{3.5-}$	I₇₄	$[2b4m7t]^{4-}$	I₇₅	$[2b3m8t]^{4.5-}$
I₇₆	$[2b2m9t]^{5-}$	I₇₇	$[2b1m10t]^{5.5-}$	I₇₈	$[2b11t]^{6-}$
I₇₉	$[1b12m]^{1-}$	I₈₀	$[1b11m1t]^{1.5-}$	I₈₁	$[1b10m2t]^{2-}$
I₈₂	$[1b9m3t]^{2.5-}$	I₈₃	$[1b8m4t]^{3-}$	I₈₄	$[1b7m5t]^{3.5-}$
I₈₅	$[1b6m6t]^{4-}$	I₈₆	$[1b5m7t]^{4.5-}$	I₈₇	$[1b4m8t]^{5-}$
I₈₈	$[1b3m9t]^{5.5-}$	I₈₉	$[1b2m10t]^{6-}$	I₉₀	$[1b1m11t]^{6.5-}$
I₉₁	$[1b12t]^{7-}$				